A Bio-inspired Dark Adaptation Framework for Low-light Image Enhancement

Fang Lei*†
*Guangdong University of Petrochemical Technology, Maoming, China
†School of Computer Science, University of Lincoln, Lincoln, UK
flei@lincoln.ac.uk

***Abstract*—In low light conditions, image enhancement is critical for vision-based artificial systems since details of objects in dark regions are buried. Moreover, enhancing the low-light image without introducing too many irrelevant artifacts is important for visual tasks like motion detection. However, conventional methods always have the risk of "bad" enhancement. Nocturnal insects show remarkable visual abilities at night time, and their adaptations in light responses provide inspiration for low-light image enhancement. In this paper, we aim to adopt the neural mechanism of dark adaptation for adaptively raising intensities whilst preserving the naturalness. We propose a framework for enhancing low-light images by implementing the dark adaptation operation with proper adaptation parameters in R, G and B channels separately. Specifically, the dark adaptation in this paper consists of a series of canonical neural computations, including the power law adaptation, divisive normalization and adaptive rescaling operations. Experiments show that the proposed bio-inspired dark adaptation framework is more efficient and can better preserve the naturalness of the image compared to existing methods.**

***Index Terms*—Bio-inspired dark adaptation, low-light image enhancement, adaptive intensity transformation, canonical neural computations.**

I. Introduction

The enhancement of low-light images is essential for vision-based autonomous robots navigating under low illumination [1]. This is because the low-light images perceived by the robots are usually with low intensity and low contrast, which brings challenges for visual tasks like motion detection. Therefore, enhancing the low-light image becomes very important for detecting faint movements in low light conditions. Moreover, motion detection relies on extracting luminance changes [2], [3], and image enhancement methods should not introduce too many unwanted artifacts or should prevent serious lightness or contrast distortion to protect the original motion information. This indicates that the preservation of the naturalness [4] of the image is important for enhancement methods.

For enhancement processing of low-light images, intensity transformation and image denoising are two highlighted aspects. The former aims to implement nonlinear operations to achieve raising the intensity of the dark pixel. The latter emphasizes the reduction of noise produced by the intensity amplification processing. Specifically, intensity amplification is a crucial step in disclosing details buried in dark regions. Here, we focus on adaptively raising intensities to overcome the problem of overenhancement and preserve luminance naturalness.

Unlike human eyes, nocturnal insects' eyes still possess remarkable visual abilities even though illumination levels are extremely low [5]. The dark adaptation in insects' visual systems can explain why they can see color and detect faint movements in very dim environments [6]. For example, the amplitude of the photoreceptor responses ("bumps") in the nocturnal species is about five times the amplitude of those in the day-active species due to higher phototransduction and membrane gains [7], [8]. Hence, the underlying neural mechanisms of dark adaptation may provide us with useful solutions to adaptively raise intensities.

Although there are various types of low-light image enhancement methods [9]–[13], such as the histogram-based method [9], the Retinex based method [11], the gradient-based method [13], etc, these methods mainly rely on the statistical information of intensities, the estimation of illumination, or other fusion information like the gradient. However, they do not consider the ever-changing illumination situations, especially for dim-light scenes with motions, which is required to raise the intensity adaptively as well as reduce the distortion.

For dark adaptations, biological researches are devoted to building plausible models to interpret the results of electrophysiological experiments, which can better explain the relationship between the captured photons and the response amplitude. Correspondingly, a lot of models were proposed for explaining the adaptations of receptors in different aspects, including Stevens' psychophysical power law adaptation mechanism [14], [15], the shunting synaptic inhibition mechanism [16], [17] and canonical neural computations [18], [19], etc. The phototransduction process is very complex, and the complete mechanisms underlying photoreceptors' dark adaptation remain unclear. Nonetheless, the exploration of nocturnal vision mechanisms is always a promising way to develop effective and efficient image enhancement algorithms.

In this paper, we propose a bio-inspired low-light image enhancement method, involving the dark adaptation processing in R, G and B channels. The dark adaptation is composed of a series of canonical neural computations, and the adaptation parameter in each color channel is related to the differ-

This work was supported in part by the EU HORIZON 2020 Project ULTRACEPT under Grant 778062, in part by the EU HORIZON 2020 Project STEP2DYNA under Grant 691154.

ent wavelength photoreceptor cell. The proposed bio-inspired adaptation method can not only adaptively raise intensities but also preserve the naturalness. The main contributions of this work are: 1) a dark adaptation based framework is proposed for low-light image enhancement, which consists of a series of canonical neural computations; 2) combining the psychophysical power law with the photoreceptor's response properties to different wavelengths of light during the application of dark adaptation for enhancing color image; 3) comprehensive analysis of parameters of the model and quantitative comparison of performance on image quality.

The remainder of this paper is organized as follows. Section II introduces the proposed bio-inspired dark adaptation framework. Section III reports comprehensive experimental results as well as performance comparisons with existing methods on the low light image dataset. Section IV presents the discussion. Finally, we conclude this chapter in Section V.

II. Bio-inspired Dark Adaptation Framework

In this section, we present the proposed bio-inspired dark adaptation framework. The key idea of the dark adaptation is to adaptively raise the intensities of dark pixels by a series of canonical neural computations. Given an input image, it is first sampled into three channels, that is, converted to the red (R), green (G), and blue (B) channel images. As shown in Fig. 1, the input image implements the dark adaptation in three separate channels to enhance the color components. It is

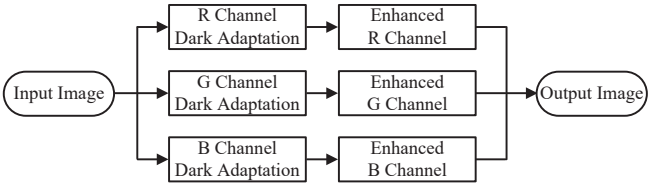

Fig. 1. Proposed dark adaptation framework for low light image enhancement. The red (R), green (G), and blue (B) components of the input image are processed with the dark adaptation in three separate channels. Note that each channel has a different adaptation parameter.

worthy to note that the dark adaptation processing within the three color channels has different adaptation parameters. This is because the three color channels correspond to the three types of photoreceptor cells which are sensitive to light with different wavelengths. Finally, the final output image can be obtained by combining the enhanced images from the three color channels.

The proposed dark adaptation consists of a series of canonical neural computations, as illustrated in Fig. 2. It involves the power law adaptation, divisive normalization and adaptive rescaling operations. First, the power law operation compresses the input intensity into a narrow range. Then, the divisive normalization adaptively maps the power law output into a range of $0 \sim 1$ controlled by the average intensity of the input image. Finally, the normalized output is remapped by adaptive rescaling operation, which can guarantee the maximum transmission of information. In the following, more

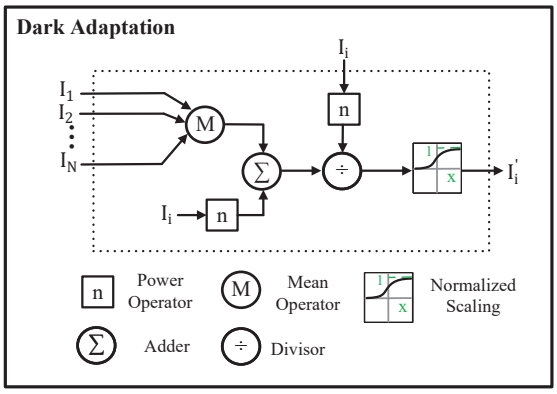

Fig. 2. Schematic illustration of the proposed dark adaptation. There are N cells that correspond to N pixels in the input image, denoted by $I_1 \sim I_N$. n denotes the sensation parameter, and its value depends on the wavelength of perceived light. I_i and $I_i^{'}$ indicate the ith cell and its enhanced output after the dark adaptation processing. For clear illustration, we only give one cell's enhanced result.

details about these neural computations mentioned above are introduced as follows.

A. Power Law Adaptation

For power law adaptation, the famous Stevens' psychophysical power law is deduced mathematically from the Weber-Fechner logarithmic law [14]. Moreover, many researchers claimed that the power law system could adjust its effective adaptation timescale to the environment [20]. The functionality of the power law adaptation is able to compress the physical stimuli into a specific range of perceived intensities by the different parameters of power. The classical power law equation is given by [14],

$$\psi = a \cdot (I - I_0)^n \tag{1}$$

where ψ is the perceived intensity, I is the physical intensity, and a, I_0 and n are constants. Note that the exponent n is related to the sensory system. Here, the value of n is related to the color channel. This power law equation describes relations between sensation magnitude and stimulus strength ranging from zero to increased strength with an upper limit of 255. We set $a = 1$ and $I_0 = 0$, then Eq. (1) has the simplest form $\psi = I^n$. The response amplitude is correspondingly only determined by the adaptation parameter n. In many invertebrate photoreceptors, the intensity/response functions are generally fitted with n less than one [21]. Hence, we display the perceived intensity results resulting from the adaptation parameter n in the range of $0.1 \sim 0.9$ (see Fig. 3). During the processing of dark adaptation, the perceived intensities in three color channels are given by,

$$\psi_R = I_R^{n_r} \tag{2a}$$
$$\psi_G = I_G^{n_g} \tag{2b}$$
$$\psi_B = I_B^{n_b} \tag{2c}$$

where the value of n_r, n_g and n_b relates to the sensation parameters of long-, medium-, and short- wavelength pho-

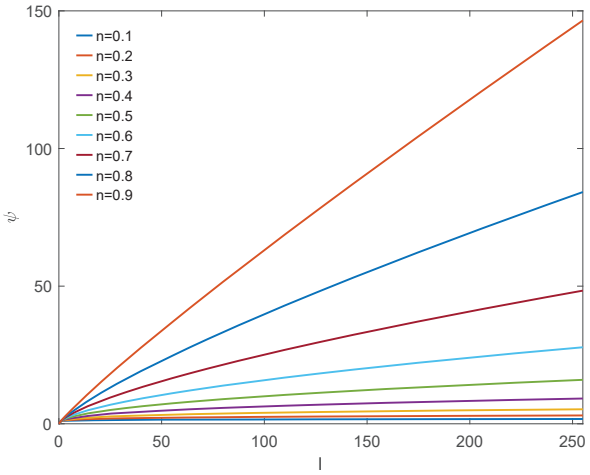

Fig. 3. The perceived intensity ψ for different values of the adaptation parameter n (refer to Eq. (1), $a = 1$, $I_0 = 0$).

toreceptor cells, responding to red light (620–750 nm), green light (495-570 nm) and blue light (450-475 nm). To determine the suitable parameters, we calculate the root-mean-square (RMS) level of the absolute difference image between the output image (power law operation for dark image) and the reference image since the RMS can be used to estimate the transformation biases [22]. We choose four groups of parameters to calculate the RMS. Each group has six different combinations of n_r, n_g and n_b, and the minimum value of RMS corresponds to the optimal combination. More details on choosing the adaptation parameters n_r, n_g and n_b are presented as follows.

Fig. 4 shows the reference image and the dark image. First, the reference image $R(x, y)$ and the dark image $I(x, y)$

(a) (b)

Fig. 4. The same scenes are captured by a GoPro camera under different illumination conditions. (a) Reference image (normal illumination). (b) Dark image (low illumination).

are converted into R, G and B channel images separately (i.e., $R_c(x, y), I_c(x, y), c \in (R, G, B)$). Then, the color components of dark image are transformed by the power law operation (see Eq. (2a-2c)) producing new images $\psi_c(x, y)$. Finally, the average RMS ($\overline{\text{RMS}}$) on the three color channels is computed by

$$\overline{\text{RMS}} = \frac{1}{3}\sum_{c=1}^{3}\sqrt{\frac{1}{M*N}\sum_{x=1}^{M}\sum_{y=1}^{N}\left|\psi_c(x, y) - R_c(x, y)\right|^2} \quad (3)$$

where M and N denote the number of rows and columns of the input image. As the fitted value of the adaptation parameter in some invertebrate photoreceptors is around 0.5 [21], the four groups of parameters are chosen including 0.5 to calculate the $\overline{\text{RMS}}$, as shown in Table I. From Table I, we can see that the optimal combination in each group has the lowest value of $\overline{\text{RMS}}$ and the value of n_r is the largest among the three parameters. It implies that the longer wavelengths of photoreceptor cells correspond to the larger n. However, the $\overline{\text{RMS}}$ only reflects the average transformation biases of R, G and B channels, which does not consider the interactions among the three channels. Further analysis of the four optimal combinations is given below.

B. Divisive Normalization

Divisive normalization can model the contrast gain control by a nonlinear operator, which is a suitable canonical computational model for processing sensory information underlying adaptation [18], [23], [24]. For normalization of the neural computation, the responses of neurons are divided by a common factor that typically includes the summed activity of a pool of neurons [18]. There are many divisive normalization models proposed for achieving gain control in the past twenty years [24]–[26]. They mostly aim to establish a connection between the gain control and the statistical properties of natural sensory stimuli [24]. However, how the component like the feedforward component in the divisive normalization model performs better in enhancing low light image data lacks further exploration.

Combining the characteristics of the self-shunting model [21], [27] and the normalization model of the odorant receptor [18], [28], we design a new divisive normalization processor in the proposed dark adaptation. This is because the perceived intensity produced by the power law operation needs to be adaptively mapped into the range of $0 \sim 1$ for further canonical computation. Compared with the traditional normalization model [18], the proposed normalization processor simply utilizes the average intensity of inputs to control the normalization output instead of the power law output of the average intensity. The background light intensity of the input as a controlling factor in the normalization model can better reflect the real illumination conditions.

Here, the designed divisive normalization processor can be mathematically described by,

$$\psi'_R = \frac{I_R^{n_r}}{I_R^{n_r} + I_{m_R}} = \frac{\psi_R}{\psi_R + I_{m_R}} \quad (4a)$$

$$\psi'_G = \frac{I_G^{n_g}}{I_G^{n_g} + I_{m_G}} = \frac{\psi_G}{\psi_G + I_{m_G}} \quad (4b)$$

$$\psi'_B = \frac{I_B^{n_b}}{I_B^{n_b} + I_{m_B}} = \frac{\psi_B}{\psi_B + I_{m_B}} \quad (4c)$$

where ψ'_R, ψ'_G and ψ'_B denote the normalized sensation magnitude output. And, I_{m_R}, I_{m_G} and I_{m_B} are the averaged intensities with respect to the three color channels. They are able to control the response gain as an additive term in the

TABLE I
THE $\overline{\text{RMS}}$ OF FOUR GROUPS OF PARAMETERS, AND EACH GROUP HAS SIX COMBINATIONS. THE OPTIMAL COMBINATION IN EACH GROUP IS HIGHLIGHTED IN BOLD, WHICH HAS THE LOWEST VALUE OF $\overline{\text{RMS}}$.

n_r, n_g, n_b	$\overline{\text{RMS}}$	n_r, n_g, n_b	$\overline{\text{RMS}}$	n_r, n_g, n_b	$\overline{\text{RMS}}$	n_r, n_g, n_b	$\overline{\text{RMS}}$
0.9,0.5,0.1	**96.65**	**0.8,0.5,0.2**	**99.99**	**0.7,0.5,0.3**	**102.13**	**0.6,0.5,0.4**	**103.41**
0.5, 0.1, 0.9	101.00	0.5, 0.2, 0.8	102.56	0.5, 0.3, 0.7	103.53	0.5, 0.4, 0.6	104.00
0.1, 0.9, 0.5	99.37	0.2, 0.8, 0.5	101.74	0.3, 0.7, 0.5	103.20	0.4, 0.6, 0.5	103.93
0.9, 0.1, 0.5	96.96	0.8, 0.2, 0.5	100.27	0.7, 0.3, 0.5	102.36	0.6, 0.4, 0.5	103.55
0.5, 0.9, 0.1	98.73	0.5, 0.8, 0.2	101.17	0.5, 0.7, 0.3	102.73	0.5, 0.6, 0.4	103.64
0.1, 0.5, 0.9	101.33	0.2, 0.5, 0.8	102.86	0.3, 0.5, 0.7	103.77	0.4, 0.5, 0.6	104.15

denominator. It is worthy to note that the additive term plays an important role in controlling the normalized outputs, which can be verified by the subfigures in Fig. 5.

Fig. 5 displays the divisive normalization outputs for the four optimal combinations of parameters that have been mentioned in Section II-A. Given a specific value for I_{m_R}, I_{m_G} and I_{m_B}, the divisive normalization outputs are presented, as shown in Fig. 5(a), (b) and (c). Note that the average intensity of each color channel is set with the same value ($I_{m_R} = I_{m_G} = I_{m_B} = I_m$), and the input I from the three color channels is in the range of $0 \sim 255$. From Fig. 5(a) to Fig. 5(c), we can see that the normalization output becomes larger and the curve at low values becomes steeper when the average intensity decreases for the four optimal combinations of parameters. This indicates that the divisive normalization operation is effective in raising the intensities of dark pixels. Additionally, we have found that the outputs corresponding to the fourth combination (the last row) have the least variance among the R, G and B channels compared to the other three combinations (rows one to three). Therefore, to keep more consistent of the color components in the final enhanced images, we choose the fourth combination $n_r = 0.6$, $n_g = 0.5$ and $n_b = 0.4$ as useful parameters in our application.

The goal of the divisive normalization processor is to map the result of the compressed data from power law operation to the range of $0 \sim 1$. Although this normalization operation indeed raises intensities for dark pixels, the responses cannot achieve maximized transmission as the produced maximum output is varied when the average intensity changes. To address this problem, the adaptive rescaling operation [29] is required after the divisive normalization operation. More details are described as follows.

C. Adaptive Rescaling

The rescaling operation can match the dynamic range of responses to that of the inputs when the dynamic range of inputs changes [29]. It ensures the adaptation of visual responses to the mean light level, even though there are fluctuations around the mean. The adaptive rescaling process in the three color channels is mathematically given by,

$$I_c{}' = \frac{\psi_c{}' - min\left(\psi_c{}'\right)}{max\left(\psi_c{}'\right) - min\left(\psi_c{}'\right)} \tag{5}$$

where $I_c{}', c \in (R, G, B)$ denotes the rescaled output for the three color components. It is worthy to note that $max\,(x)$ and $min\,(x)$ indicate the implementations of the maximum and minimum operation.

Fig. 6 shows the rescaling results under different average intensities, where the contrasts of inputs with low intensities are greatly increased. The rescaling outputs in Fig. 6 are shown more adaptive than those without ones (see Fig. 5), which indicates that the rescaling operation can maximize the transmitted information. This also explains the reason why it is needed after the divisive normalization processing.

III. Experiments

A. Experimental Setup

1) **Data Set:** The proposed bio-inspired dark adaptation framework is evaluated on a real low-light image dataset. The dataset contains static images with a resolution of 3000×4000 and images from video clips with a resolution of 960×1280. All images were captured by a GoPro camera under natural or artificial illumination conditions in indoor environments.

2) **Evaluation Metric:** For preserving the naturalness of the image during the enhancement processing, no light source should be introduced to the scene, no halo effect should be added and no blocking effect should be amplified [30]. The naturalness of the image is also defined as: the global ambience of the image should not be changed seriously and the direction of the light source should not be altered obviously [4]. Since the naturalness of an enhanced image is related to the relative order of lightness in different local areas [4], we therefore employ lightness order error (LOE) to quantitatively measure the lightness distortion of enhanced results. The lower LOE indicates that the enhancement better preserves the naturalness of illumination [11]. The definition of LOE is mathematically given by [12],

$$LOE = \frac{1}{m}\sum_{x=1}^{m} RD\,(x) \tag{6}$$

where m is the pixel number, $RD\,(x)$ is the relative order difference of the lightness between the reference image and

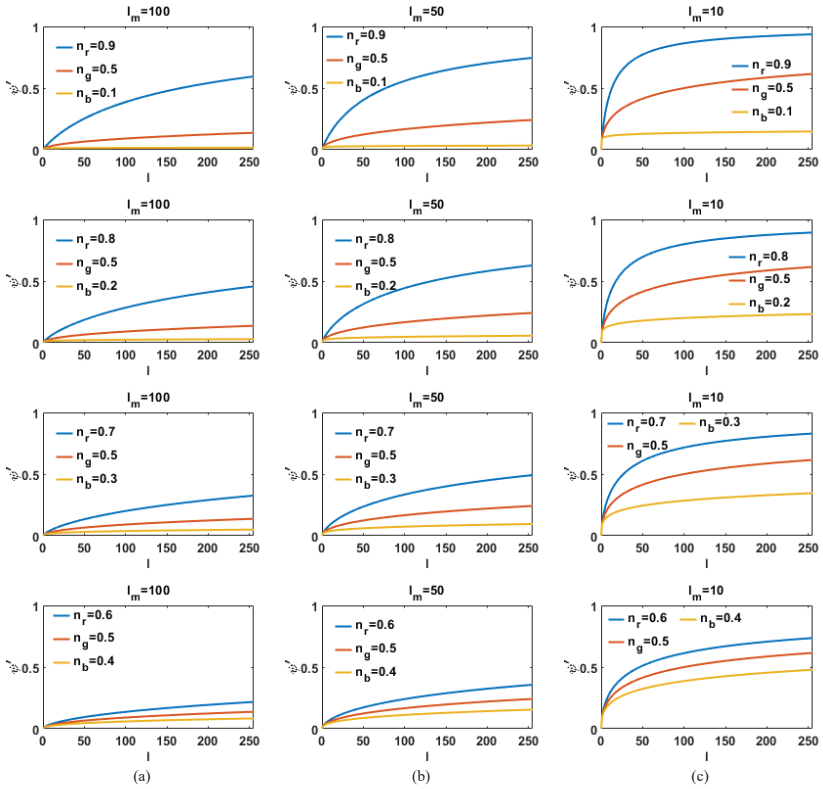

Fig. 5. The divisive normalization operation for different value of the additive term I_{m_R}, I_{m_G} and I_{m_B} (refer to Eq. 4). Here, we set the average intensity in each color channel (R, G, and B) with the same value, $I_{m_R} = I_{m_G} = I_{m_B} = I_m$. (a) $I_m = 100$. (b) $I_m = 50$. (c) $I_m = 10$.

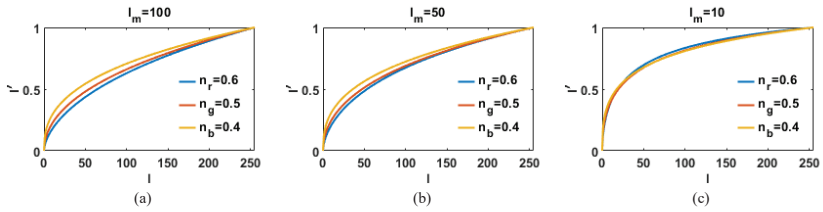

Fig. 6. The results of adaptive rescaling operation with respect to the adaptation parameters $n_R = 0.6$, $n_G = 0.5$ and $n_B = 0.4$ (refer to Eq. 5).

the enhanced version of the low-light image for pixel x, which is defined as follows:

$$RD\left(x\right) = \frac{1}{m}\sum_{y=1}^{m} U\left(Q\left(x\right), Q\left(y\right)\right) \oplus \left(U\left(Q_r\left(x\right)\right), Q_r\left(y\right)\right) \tag{7}$$

where the function $U(p, q)$ returns 1 if $p >= q$, 0 otherwise, $\oplus$ stands for the exclusive-or operator. $Q(x)$ and $Q_r(x)$ denote the lightness component at location x of the enhanced and reference image respectively, which are the maximum values among R, G and B channels. However, the LOE is highly complex computationally. Hence, a down-sampling is used to reduce the complexity of computing LOE [12]. Specifically, all images are down-sampled to a fixed size 100×100 by collecting 100 rows and columns evenly.

According to the definition of LOE, we can find that its value depends on the lightness component of the reference image (Q_r). In [11], it has pointed out that using the low-light input as the reference is problematic since there exists an extreme case that the LOE is 0 when no enhancement is performed. However, they adopt the HDR [10] result as the reference which is a groundtruth produced by the artificial enhancement algorithm. For the sake of objectiveness, we use the image of the same scene captured under higher illuminations as the reference with respect to the dark and very dark images.

***2)* Implementation:** The proposed bio-inspired dark adaptation framework was implemented in Matlab environment on a standard laptop with a 1.80GHz Intel Core i5 CPU and 16.00GB RAM memory. The adaptation parameters n_R, n_G and n_B are set with 0.6, 0.5 and 0.4, which have been explained in Section II.

B. Comparison on Real Low-Light Dataset

To evaluate the performance of the proposed bio-inspired dark adaptation framework, we compare it with existing low light image enhancement methods, including Adaptive Contrast-Limited Adaptive Histogram Equalization (CLAHE), Matlab HDR (High-Dynamic Range) image tone mapping (HDR), Illumination Estimation based method (LIME) [11], Bio-Inspired Multi-Exposure Fusion method (BIMEF) [12] and Gradient-based method (Tanaka's) [13]. Note that the codes of LIME, BIMEF and Tanaka's are downloaded from the authors' websites using default parameters. For CLAHE and HDR, we use the *adapthisteq* and the *tonemap* function integrated in the Matlab toolbox applying default parameters. Particularly, the operation of CLAHE is executed on the L channel by first converting it from the RGB colorspace to the LAB one and then converting the processed LAB back to the RGB colorspace.

The sample images of the tested low-light dataset are shown in Fig. 7. There are twelve images recording four different scenes. Each scene includes three images captured under different levels of illumination. Specifically, the images captured under dark and very dark environments are tested images utilized to compare the performance between the proposed method and other enhancement methods, while the images captured under higher illuminations are regarded as the reference images for calculating the LOE.

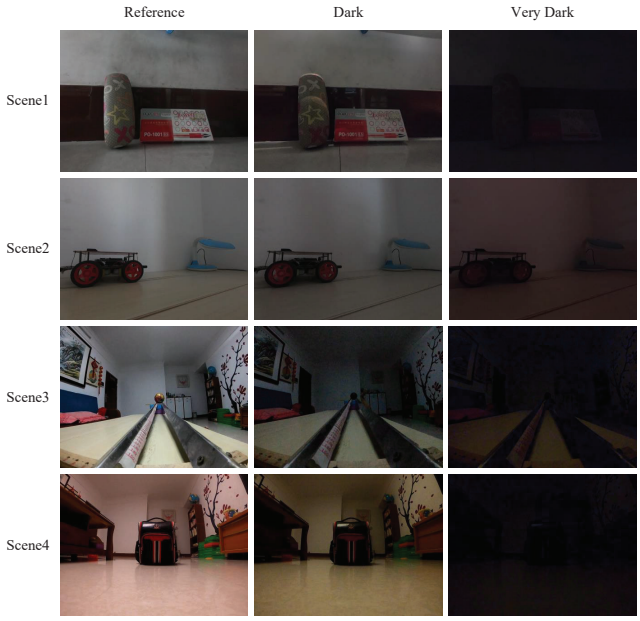

Fig. 7. Sample images in the low-light image dataset. From the first column to the third column, images are captured under different levels of illumination. The scenes recorded by the images in each row are the same. Specifically, scene1 and scene2 are static images while scene3 and scene4 are images from video clips. Note that images in the first column are captured under higher illumination, which is used in the evaluation experiments as the reference images for the dark and very dark scenes in the second and the third columns.

Fig. 8 provides the visual comparison among the competitors on different scenes of the low-light image dataset where the dark inputs are displayed in the second column and the third column in Fig. 7. From Fig. 8, we can observe that the proposed method has better visual performance when the enhanced image does not implement further denoising processing compared with other competitors, especially in very dark conditions.

Table II shows the LOE numbers of all the competitors on the low-light image dataset. As can be seen from the numbers in Table II, the proposed method has the lowest average LOE which significantly outperforms others.

Table III gives the average running time comparison of the six methods on the low-light image dataset where the proposed method costs the least average running time. It demonstrates that the proposed method is much more efficient in computation than other competitors.

IV. Discussion

In the above section, we have proposed a bio-inspired dark adaptation framework for low-light image enhancement. The experiments showed that the proposed method performs better visual performance and the results are closer to the references than the others when challenged with low-light images. However, the proposed method only considers raising the intensities but does not deal with the inevitable noise problem. In [5], [7], the bio-inspired night-vision algorithms use spatio–temporal summation neural strategy to reduce noise. Therefore, for low-light image enhancement, it is worth combing other neural strategies together in future work to obtain more pleasant visual performances.

V. Conclusion

To summarize, we have proposed a low-light image enhancement method which involves dark adaptation processing in three color channels. The key to the dark adaptation is to adaptively raise the intensities of dark pixels by integrating a series of canonical neural computations. Moreover, the important parameters for power law adaptation are analyzed in detail for the three color channels. Experimental results on the low-light dataset have demonstrated its effectiveness and efficiency in enhancing intensities and contrasts as well as preserving the naturalness. It therefore can feed the vision-based application like motion detection in low light environments as a positive enhancement method.

In our future work, we will integrate other neural mechanisms with the proposed model for further denoising to obtain better visual performance. Additionally, it can be combined with other techniques for motion detection in low light conditions.

References

[1] M. Aladem, S. Baek, and S. A. Rawashdeh, "Evaluation of image enhancement techniques for vision-based navigation under low illumination," *Journal of Robotics*, vol. 2019, 2019.

[2] R. Behnia, D. A. Clark, A. G. Carter, T. R. Clandinin, and C. Desplan, "Processing properties of on and off pathways for drosophila motion detection," *Nature*, vol. 512, no. 7515, p. 427, 2014.

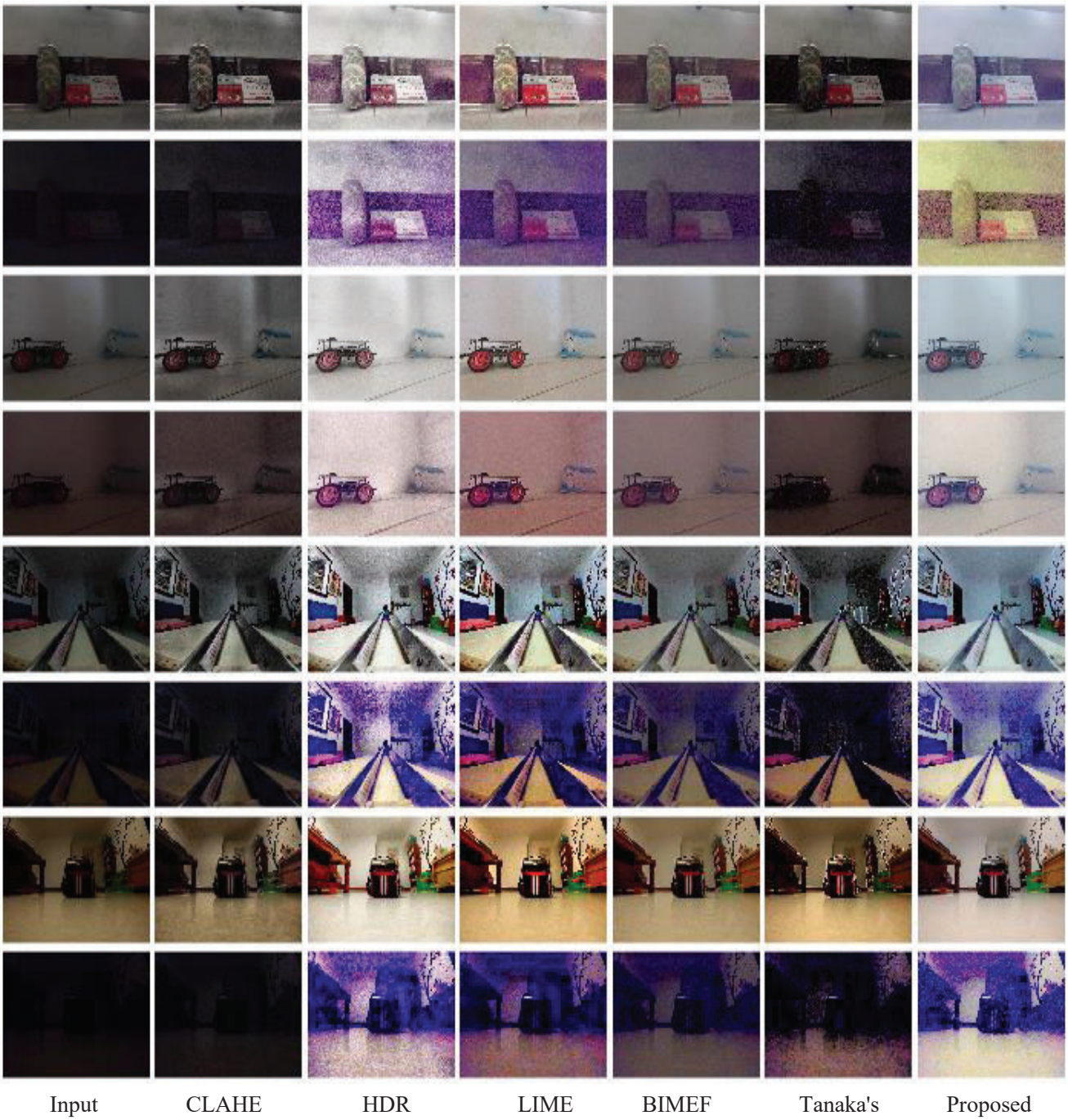

Fig. 8. Visual comparison among the competitors on the low-light image dataset.

TABLE II
QUANTITATIVE PERFORMANCE COMPARISON ON THE LOW-LIGHT IMAGE DATASET IN TERMS OF LOE. LOE HAS A FACTOR 10^3. **THE LOWER THE LOE IS, THE BETTER THE ENHANCEMENT PRESERVES THE NATURALNESS OF ILLUMINATION**.

Method	Scene1 Dark	Scene1 Very Dark	Scene2 Dark	Scene2 Very Dark	Scene3 Dark	Scene3 Very Dark	Scene4 Dark	Scene4 Very Dark	Ave. **LOE**
CLAHE	2.162	2.808	2.592	1.038	2.216	2.450	**2.663**	1.426	2.169
HDR	1.858	2.479	2.744	0.988	2.611	1.930	3.420	2.488	2.315
LIME	2.032	2.058	2.741	1.274	2.728	1.913	3.170	2.194	2.264
BIMEF	**1.625**	**1.379**	2.474	0.452	2.028	1.171	2.999	1.571	1.712
Tanaka's	1.695	1.493	2.723	0.822	2.675	1.174	3.027	1.856	1.933
Proposed	1.675	1.441	**2.392**	**0.297**	**1.482**	**1.001**	2.924	**1.260**	**1.559**

TABLE III
AVERAGE RUNNING TIME COMPARISON OF THE SIX ENHANCEMENT METHODS ON THE LOW-LIGHT IMAGE DATASET. THE SIZES OF IMAGES ARE 1280 PIXELS (HORIZONTAL) $\times$ 960 PIXELS (VERTICAL) AND 4000 PIXELS (HORIZONTAL) $\times$ 3000 PIXELS (VERTICAL).

	CLAHE	HDR	LIME	BIMEF	Tanaka's	Proposed
Time (s)	6.160	8.231	4.769	5.294	35.441	**1.182**

[3] F. Lei, Z. Peng, V. Cutsuridis, M. Liu, Y. Zhang, and S. Yue, "Competition between on and off neural pathways enhancing collision selectivity," in *2020 International Joint Conference on Neural Networks (IJCNN)*. IEEE, 2020, pp. 1–8.

[4] S. Wang, J. Zheng, H.-M. Hu, and B. Li, "Naturalness preserved enhancement algorithm for non-uniform illumination images," *IEEE Transactions on Image Processing*, vol. 22, no. 9, pp. 3538–3548, 2013.

[5] E. Warrant, M. Oskarsson, and H. Malm, "The remarkable visual abilities of nocturnal insects: neural principles and bioinspired night-vision algorithms," *Proceedings of the IEEE*, vol. 102, no. 10, pp. 1411–1426, 2014.

[6] E. J. Warrant, "The remarkable visual capacities of nocturnal insects: vision at the limits with small eyes and tiny brains," *Philosophical Transactions of the Royal Society B: Biological Sciences*, vol. 372, no. 1717, p. 20160063, 2017.

[7] ——, "Superior visual performance in nocturnal insects: neural principles and bio-inspired technologies," in *Bioinspiration, Biomimetics, and Bioreplication 2016*, vol. 9797. International Society for Optics and Photonics, 2016, p. 979703.

[8] R. V. Frolov and I. I. Ignatova, "Electrophysiological adaptations of insect photoreceptors and their elementary responses to diurnal and nocturnal lifestyles," *Journal of Comparative Physiology A*, vol. 206, no. 1, pp. 55–69, 2020.

[9] E. D. Pisano, S. Zong, B. M. Hemminger, M. DeLuca, R. E. Johnston, K. Muller, M. P. Braeuning, and S. M. Pizer, "Contrast limited adaptive histogram equalization image processing to improve the detection of simulated spiculations in dense mammograms," *Journal of Digital imaging*, vol. 11, no. 4, p. 193, 1998.

[10] P. Sen, N. K. Kalantari, M. Yaesoubi, S. Darabi, D. B. Goldman, and E. Shechtman, "Robust patch-based hdr reconstruction of dynamic scenes." *ACM Trans. Graph.*, vol. 31, no. 6, pp. 203–1, 2012.

[11] X. Guo, Y. Li, and H. Ling, "Lime: Low-light image enhancement via illumination map estimation," *IEEE Transactions on image processing*, vol. 26, no. 2, pp. 982–993, 2016.

[12] Z. Ying, G. Li, and W. Gao, "A bio-inspired multi-exposure fusion framework for low-light image enhancement," *arXiv preprint arXiv:1711.00591*, 2017.

[13] M. Tanaka, T. Shibata, and M. Okutomi, "Gradient-based low-light image enhancement," in *2019 IEEE International Conference on Consumer Electronics (ICCE)*. IEEE, 2019, pp. 1–2.

[14] D. MacKay, "Psychophysics of perceived intensity: A theoretical basis for fechner's and stevens' laws," *Science*, vol. 139, no. 3560, pp. 1213a–1216, 1963.

[15] J. C. Stevens and L. E. Marks, "Stevens power law in vision: exponents, intercepts, and thresholds," *Fechner Day*, vol. 99, pp. 82–87, 1999.

[16] G. Sperling, "Model of visual adaptation and contrast detection," *Perception & Psychophysics*, vol. 8, no. 3, pp. 143–157, 1970.

[17] S. J. Mitchell and R. A. Silver, "Shunting inhibition modulates neuronal gain during synaptic excitation," *Neuron*, vol. 38, no. 3, pp. 433–445, 2003.

[18] M. Carandini and D. J. Heeger, "Normalization as a canonical neural computation," *Nature Reviews Neuroscience*, vol. 13, no. 1, pp. 51–62, 2012.

[19] T. Brosch and H. Neumann, "Computing with a canonical neural circuits model with pool normalization and modulating feedback," *Neural computation*, vol. 26, no. 12, pp. 2735–2789, 2014.

[20] B. Wark, B. N. Lundstrom, and A. Fairhall, "Sensory adaptation," *Current opinion in neurobiology*, vol. 17, no. 4, pp. 423–429, 2007.

[21] T. Matić and S. Laughlin, "Changes in the intensity-response function of an insect's photoreceptors due to light adaptation," *Journal of comparative physiology*, vol. 145, no. 2, pp. 169–177, 1981.

[22] N. G. Paulter, D. R. Larson, and J. J. Blair, "The ieee standard on transitions, pulses, and related waveforms, std-181-2003," *IEEE Transactions on Instrumentation and Measurement*, vol. 53, no. 4, pp. 1209–1217, 2004.

[23] T. Ohshiro, D. E. Angelaki, and G. C. DeAngelis, "A normalization model of multisensory integration," *Nature neuroscience*, vol. 14, no. 6, pp. 775–782, 2011.

[24] A. A. Lazar, N. H. Ukani, and Y. Zhou, "Sparse identification of contrast gain control in the fruit fly photoreceptor and amacrine cell layer," *The Journal of Mathematical Neuroscience*, vol. 10, no. 1, pp. 1–35, 2020.

[25] O. Schwartz and E. P. Simoncelli, "Natural sound statistics and divisive normalization in the auditory system," *Advances in neural information processing systems*, pp. 166–172, 2001.

[26] M. Rivera-Alba, S. N. Vitaladevuni, Y. Mishchenko, Z. Lu, S.-y. Takemura, L. Scheffer, I. A. Meinertzhagen, D. B. Chklovskii, and G. G. de Polavieja, "Wiring economy and volume exclusion determine neuronal placement in the drosophila brain," *Current Biology*, vol. 21, no. 23, pp. 2000–2005, 2011.

[27] P. Skorupski and L. Chittka, "Photoreceptor spectral sensitivity in the bumblebee, bombus impatiens (hymenoptera: Apidae)," *PLoS One*, vol. 5, no. 8, p. e12049, 2010.

[28] S. R. Olsen, V. Bhandawat, and R. I. Wilson, "Divisive normalization in olfactory population codes," *Neuron*, vol. 66, no. 2, pp. 287–299, 2010.

[29] N. Brenner, W. Bialek, and R. d. R. Van Steveninck, "Adaptive rescaling maximizes information transmission," *Neuron*, vol. 26, no. 3, pp. 695–702, 2000.

[30] S. Chen and A. Beghdadi, "Natural rendering of color image based on retinex," in *2009 16th IEEE International Conference on Image Processing (ICIP)*. IEEE, 2009, pp. 1813–1816.